A Multifunctional Polymeric Nanotheranostic System Delivers Doxorubicin and Imaging Agents across the Blood–Brain Barrier Targeting Brain Metastases of Breast Cancer

Jason Li,[†,▽] Ping Cai,[†,▽] Alireza Shalviri,[†,▽] Jeffrey T. Henderson,[†] Chunsheng He,[†] Warren D. Foltz,[‡] Preethy Prasad,[†] Peter M. Brodersen,[§] Yonghong Chen,[∥] Ralph DaCosta,[∥,⊥,#] Andrew Michael Rauth,[∥,⊥] and Xiao Yu Wu*[,†]

[†]Department of Pharmaceutical Sciences, Leslie Dan Faculty of Pharmacy, University of Toronto, Toronto, Ontario M5S 3M2, Canada, [‡]Department of Radiation Oncology, Princess Margaret Cancer Centre, University Health Network, Toronto, Ontario M5G 2M9, Canada, [§]Department of Chemistry, University of Toronto, Toronto, Ontario M5S 3E5, Canada, [∥]Princess Margaret Cancer Centre, The Campbell Family Institute for Cancer Research, University Health Network, Toronto, Ontario M5G 2M9, Canada, [⊥]Department of Medical Biophysics, University of Toronto, Toronto, Ontario M5G 1L7, Canada, and [#]Techna Institute for the Advancement of Technology for Health, University Health Network, Toronto, Ontario M5G 2M9, Canada. [▽]These authors contributed equally to this work.

ABSTRACT Metastatic brain cancers, in particular cancers with multiple lesions, are one of the most difficult malignancies to treat owing to their location and aggressiveness. Chemotherapy for brain metastases offers some hope. However, its efficacy is severely limited as most chemotherapeutic agents are incapable of crossing the blood–brain barrier (BBB) efficiently. Thus, a multifunctional nanotheranostic system based on poly(methacrylic acid)–polysorbate 80-grafted-starch was designed herein for the delivery of BBB-impermeable imaging and therapeutic agents to brain metastases of breast cancer. *In vivo* magnetic resonance imaging and confocal fluorescence microscopy were used to confirm extravasation of gadolinium and dye-loaded nanoparticles from intact brain microvessels in healthy mice. The targetability of doxorubicin (Dox)-loaded nanoparticles to intracranially established brain metastases of breast cancer was evaluated using whole body and *ex vivo* fluorescence imaging of the brain. Coexistence of nanoparticles and Dox in brain metastatic lesions was further confirmed by histological and microscopic examination of dissected brain tissue. Immuno-histochemical staining for caspase-3 and terminal-deoxynucleotidyl transferase dUTP nick end labeling for DNA fragmentation in tumor-bearing brain sections revealed that Dox-loaded nanoparticles selectively induced cancer cell apoptosis 24 h post-injection, while sparing normal brain cells from harm. Such effects were not observed in the mice treated with free Dox. Treatment with Dox-loaded nanoparticles significantly inhibited brain tumor growth compared to free Dox at the same dose as assessed by *in vivo* bioluminescence imaging of the brain metastases. These findings suggest that the multifunctional nanoparticles are promising for the treatment of brain metastases.

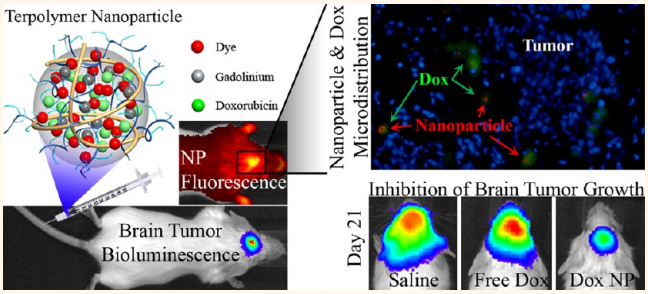

KEYWORDS: theranostic nanoparticle · multifunctional polymer · brain metastases of breast cancer · blood–brain barrier · doxorubicin · chemotherapy · polysorbate 80

Brain metastases are one of the most difficult malignancies to treat and have poor patient prognosis. They are estimated to occur in 10–30% of all cancer patients, of which 20–30% presents with solitary brain metastasis and the remainder present with multiple lesions.[1−6] While surgical resection may be possible for primary brain tumors and brain metastases with up to three lesions, whole brain radiotherapy (WBRT) is preferred for patients with multiple brain metastases due to a high risk of surgical complications including intracranial infection or brain edema. Given the significant neurotoxicity associated with WBRT, alternative noninvasive methods

* Address correspondence to xywu@phm.utoronto.ca.

Received for review February 22, 2014 and accepted October 2, 2014.

Published online October 13, 2014
10.1021/nn501069c

including chemotherapy are desirable for the treatment of brain tumors and brain metastases.[6]

Unfortunately, malignancies in the central nervous system (CNS) are notably resistant to systemic chemotherapy as many chemotherapeutic agents are incapable of efficiently crossing the blood–brain barrier (BBB).[7−11] This barrier at the capillary–CNS interface is comprised of specialized tight junctions between vascular endothelial cells which interface with associated pericytes and astrocytes to regulate the entry of nutrients and others substances to the brain. The action of drug efflux pumps such as P-glycoprotein (P-gp) or breast cancer resistance protein (BCRP) at the BBB further reduce accumulation of chemotherapeutic agents including doxorubicin (Dox) to the CNS. The vast majority of CNS drugs currently on the market must be administered at very high doses resulting in severe side effects in peripheral organs.[9]

Various approaches have been investigated to enhance drug delivery to the brain including invasive and noninvasive means.[6,12,13] Invasive approaches are expensive and associated with a high degree of patient discomfort and a high risk of complications. Noninvasive CNS drug delivery approaches using retrometabolic pro-drugs or specific drug–antibody conjugates targeting endocytic receptors on the BBB have been developed to improve treatment outcomes; however, these approaches are susceptible to loss of drug activity after modification and require complicated and expensive preparation procedures.[7,11] To mitigate this problem, nanoparticle drug carriers with a variety of targeting moieties have been investigated.[7−21]

Surface modified nanoparticulate carrier systems for noninvasive CNS drug delivery offer several advantages such as high drug loading capacity, ability to evade efflux pump action at the brain microvessels, and size-tunability. Various targeting moieties have been studied to enhance nanoparticle transport across the BBB *via* receptor-mediated pathways, including those targeting the insulin receptor,[14] transferrin receptor,[15] low density lipoprotein (LDL) receptor,[16,17] or glutathione receptor.[18] Certain surfactants, including polysorbate 80 (PS 80) have also been employed to coat nanoparticles for brain targeted drug delivery.[10,19−21] Given its low cost and approved use in many injectable pharmaceutical products,[22] PS 80 offers tremendous potential as compared to antibodies.

In a series of studies, Kreuter and co-workers[23−25] demonstrated a remarkable efficacy of Dox loaded in PS 80-coated nanoparticles for the treatment of intracranial 101/8 glioblastoma grown in rats. Being a P-gp substrate, free Dox does not penetrate across the BBB in amounts sufficient for effective chemotherapy. Intravenous administration of Dox-loaded poly(butyl cyanoacrylate) nanoparticles coated with PS 80 significantly extended the survival times of rats bearing a single brain tumor.[25] It has been demonstrated that PS 80 coated nanoparticles recruit apolipoprotein-E (ApoE) in the plasma, mimicking LDL particles which are transported cross the BBB *via* LDL receptor-mediated transcytosis due to elevated expression of these receptors on brain microvessel endothelium.[21] Later ApoE or ApoB covalently modified nanoparticles were prepared for crossing the BBB.[26−28] However, the cost and availability of lipoproteins could limit their future applications.

Recently cell-penetrating peptide-linked dendrigraft poly-L-lysine nanoparticles and arginylglycylaspartic acid (RGD)-conjugated polymer micelles have been developed and shown to exhibit antitumor efficacy in U87MG human glioblastoma xenografts.[29,30] To our knowledge, the studies of nanoparticles for drug delivery across the BBB have been limited so far to primary brain tumors such as glioblastomas. Given the vast anatomical differences between brain metastases and primary glioblastomas,[31] delivering drugs to multiple brain metastasis lesions remains very challenging.[32] In this study, a new multifunctional theranostic nanocarrier system was designed based on a terpolymer containing poly(methacrylic acid) and PS 80 covalently grafted onto starch (PMAA–PS 80-g-St), which was previously developed in our laboratory using a novel one-pot dispersion polymerization method.[33−36] The PS 80 content in the nanocarrier system was optimized to facilitate brain entry. We first examined BBB-penetration and brain accumulation of the nanoparticles containing gadolinium (Gd) and Hoechst 33342, two BBB-impermeable imaging agents, in healthy mouse brain by using magnetic resonance imaging (MRI) and confocal fluorescence microscopy, respectively. The unique nuclear staining property of Hoechst 33342 was utilized previously to demonstrate the capability of nanoparticles for delivering BBB-impermeable agent across the BBB.[37,38] The accumulation of Dox-loaded nanoparticles in a brain metastasis model of triple (estrogen, progesterone and Her2/neu receptor) negative human breast cancer was assessed by *in vivo* bioluminescent and fluorescent imaging. Microscopic localization of nanoparticles and Dox in tumor-bearing brain tissue was examined histologically using fluorescence microscopy. Terminal deoxynucleotidyl transferase dUTP nick end labeling (TUNEL) and caspase-3 immunohistochemistry was used to evaluate apoptosis in metastatic lesions following treatment with Dox-loaded nanoparticles. Longitudinal *in vivo* bioluminescence imaging of brain tumor-bearing mice was employed to assess the effect of Dox-loaded nanoparticles on tumor growth inhibition as compared to treatment with equivalent doses of free Dox. To our knowledge,

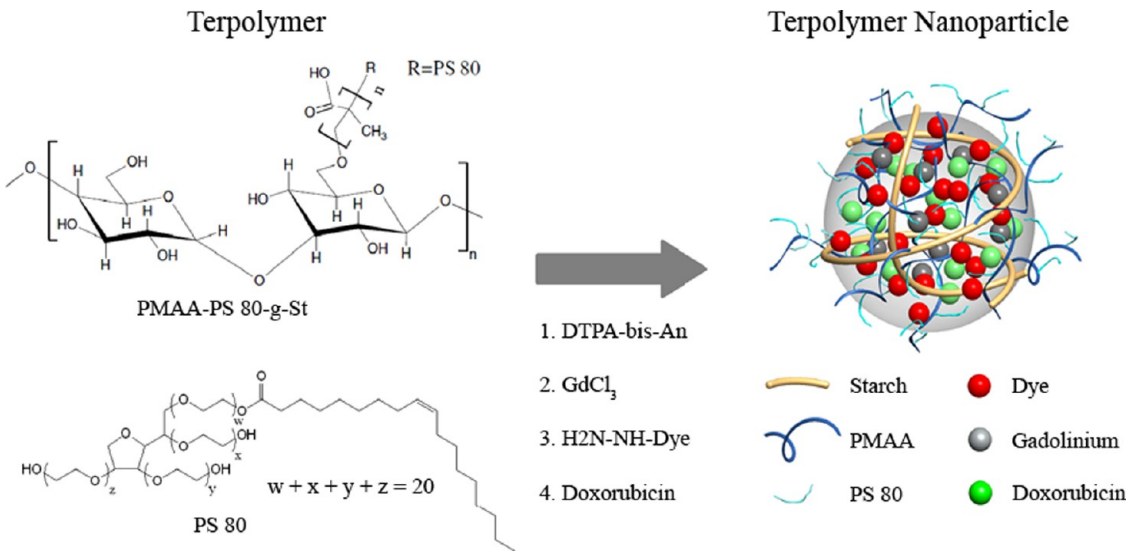

Figure 1. Structures of the terpolymer and PS 80, and a schematic diagram of the self-assembly of PMAA–PS 80-g-St terpolymer into nanoparticles upon conjugation of the fluorescent moieties, chelation with Gd^{3+} and complexation with doxorubicin.

this work represents for the first time a nanotheranostic system that has been generated to (1) specifically deliver anticancer drugs to multiple lesions of brain metastases with large to microsizes and (2) selectively destroy cancer cells while sparing normal brain cells from damage.

RESULTS AND DISCUSSION

This paper describes the investigation of a multifunctional PMAA–PS 80-g-St nanoparticulate system for the delivery of BBB-impermeable drugs and contrast agents to the brain in healthy mice and to multiple lesions of brain metastases of human breast cancer in a mouse model. The novel nanocarrier system is a single multifunctional platform with multimodal imaging and drug delivery capabilities. It can effectively coencapsulate hydrophobic moieties, cationic drug (*e.g.*, Dox) and multiple contrast agents (*e.g.*, MR contrast agent gadolinium, near-infrared (NIR) fluorescence probe HF750), enhance brain tumor accumulation, and improve *in vivo* biodistribution of drugs. While PS 80-coated nanoparticles have previously been used for the treatment of primary glioblastoma tumors,[7,25] this paper presents the first application of a multifunctional theranostic system containing covalently bound PS 80 for the diagnosis and treatment of brain metastases of breast cancer with tumor-specific cytotoxicity, a significant advance toward chemotherapy of brain metastases.

Synthesis and Characterization of PMAA–PS 80-g-St Polymer and Nanoparticles. A starch-based polymer was synthesized for the preparation of nanoparticles due to its excellent biocompatibility and biodegradability, and an abundance of reactive functional groups for further modification. Both PMAA and PS 80 are biocompatible and are widely used in Federal Drug Administration (FDA) approved pharmaceuticals. Grafting these two polymers onto the starch backbone imparted the nanocarrier system BBB-penetrating and pH-dependent drug release properties, respectively (Figure 1). This polymer was further modified with a gadolinium (Gd) chelating agent 2-(bis(2-(2,6-dioxomorpholino)ethyl)amino)-acetic acid (DTPA-bis-AN) and a near-infrared NIR fluorescence dye (H_2N-NH-HiLyteFluor 750, HF750) for dual modality *in vivo* imaging using magnetic resonance imaging (MRI) and fluorescence imaging. The PMAA–PS 80-g-St polymer was characterized by proton magnetic resonance imaging (^1H NMR) spectroscopy in 0.01 N NaOD with the peaks corresponding to starch, PMAA, and PS 80 highlighted in Figure S1 (Supporting Information). The spectrum of PS 80 is also included for comparison. The areas under the peaks at 5.1, 3.70, and 1.66 were used to calculate the molar ratio of starch, PS 80, and MAA in the final product (Table 1).

For studies in healthy mice, fluoresceinamine (FA) ($\lambda_{ex} = 496$, $\lambda_{em} = 520$) and Gd conjugation to the DTPA and HF750 modified PMAA–PS 80-g-St terpolymer resulted in the spontaneous formation of nanoparticles. Hoechst 33342-loaded nanoparticles with or without PS 80 component were formed by the addition of ethyl arachidate under sonication. The Dox-loaded nanoparticle formulation for studies in tumor-bearing mice excluded conjugation with FA because Dox autofluorescence occurs over similar wavelengths and the addition of Dox to the polymer induces nanoparticle self-assembly. The composition, size and surface charge of the nanoparticles are listed in Table 1. All nanoparticles exhibited a negative zeta potential that is favorable for biocompatibility and nanoparticle colloidal stability, especially for particles that rely on electronic repulsion forces for stability.[39] Moreover,

TABLE 1. Composition and Properties of Terpolymer Nanoparticle Formulations Loaded with Gd, HF 750, FA or HF 750 and Dox[a]

sample	Gd content (wt %)	HF 750 content (μmol/g)	FA content (μmol/g)	Dox content (wt %)	Hoechst 33342 content (mg/mL)	particle size (nm)	ξ-potential (mV)
PMAA—PS 80-g-St NP loaded with Gd, HF 750 and FA	10.2 ± 0.7	5.5 ± 0.1	22.1 ± 0.2	-	-	40.0 ± 5.5	−27.5 ± 5.2
PMAA—PS 80-g-St NP loaded with Hoechst 33342	-	-	-	-	2.5	70 ± 6.2	−40 ± 4.5
PMAA-g-St NP loaded with Hoechst 33342	-	-	-	-	2.5	70 ± 4.4	−41 ± 3.7
PMAA—PS 80-g-St NP loaded with HF 750 and Dox	-	4.3 ± 0.01	-	21.1 ± 0.3	-	61.9 ± 5.0	−38.0 ± 1.0

[a] Values shown are the means and standard deviations of the mean for $n = 3$ independent experiments. In all formulations, the feed concentrations of MAA, PS 80 and St were respectively 23.2, 1.1, and 9.2 mmol., that is, at a molar ratio of 1:0.02:0.5. Note that the mole of PS 80 was calculated based on the polymer molecular weight, while that of St and MAA was from monomer molecular weight.

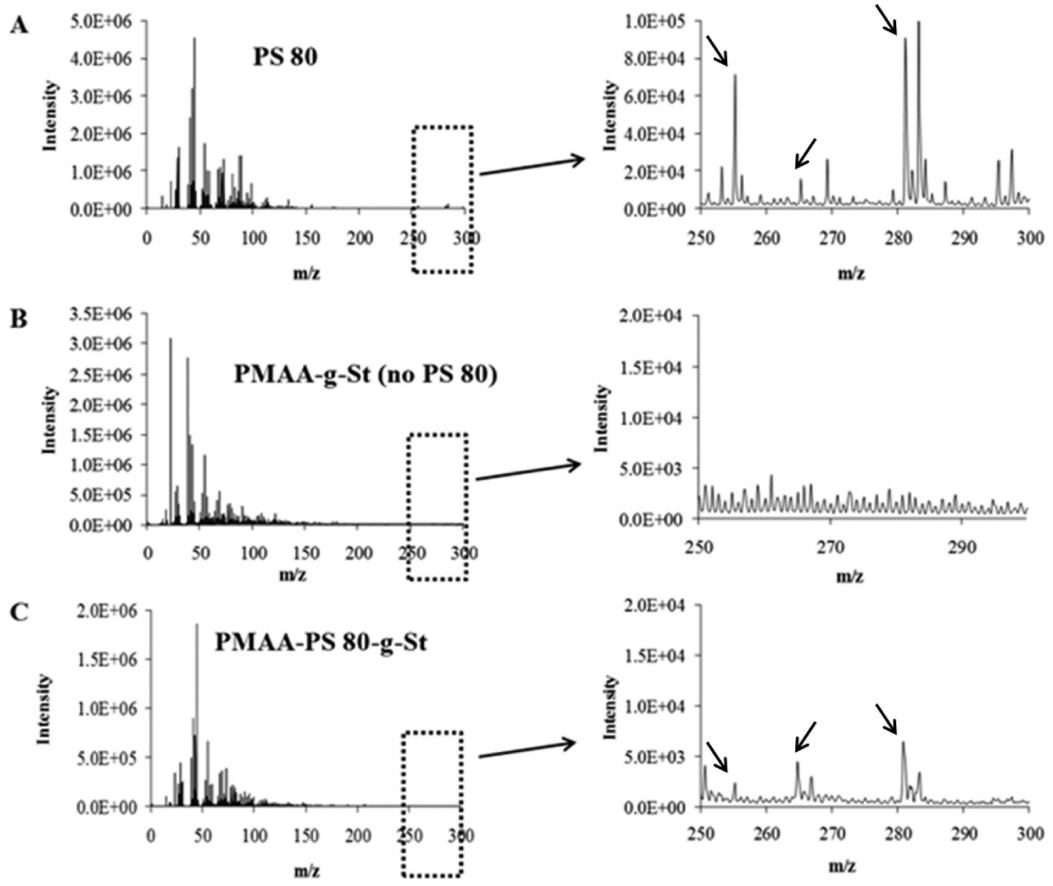

Figure 2. Negative TOF-SIMS spectra of (A) PS 80, (B) PMAA-g-St, and (C) PMAA—PS 80-g-St, in the *m/z* range of 0—300 atomic mass units. Dotted rectangles show expansion of the *y* axis by 100-fold and the *x* axis by 5-fold for the designated regions. Arrows in the right-hand side of the figure indicate PS 80 characteristic peaks.

the negative surface charge appears important for making nanoparticles nontoxic to the BBB.[40] Transmission electron microscopy (TEM) of the formulated nanoparticles showed spherical particle geometry (Figure S2, Supporting Information). Time of flight—secondary ion mass spectrometry (TOF-SIMS) confirmed the presence of covalently linked PS 80 on the nanoparticles surface as evidenced by the characteristic peaks at 255, 265, and 282 *m/z* in the negative ion mode (Figure 2). These peaks represent the series of oleic and stearic fatty acid side chains of the sorbitan molecule. These peaks were absent from the control samples lacking PS 80.

Accumulation of the PMAA—PS 80-g-St Nanoparticles in Healthy Mouse Brain. To investigate whether PMAA—PS 80-g-St nanoparticles are able to cross the BBB and enter the brain, Gd loaded nanoparticles and Hoechst 33342-loaded nanoparticles were administered intravenously to healthy Balb/c mice for *in vivo* MRI and laser scanning confocal microscopy, respectively.

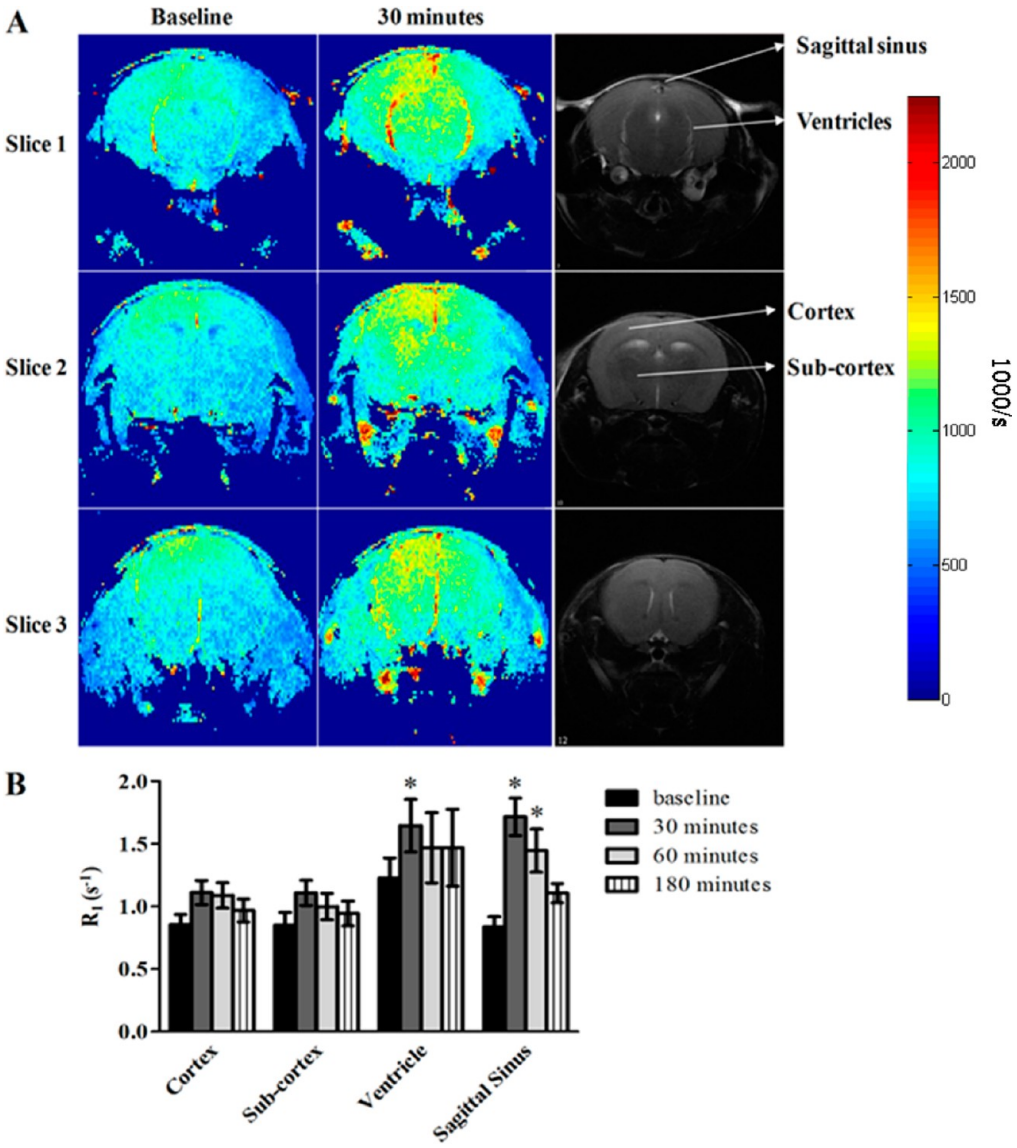

Figure 3. Quantitative MRI of brain distribution: (A) R_1 maps of Balb/c mice ($n = 3$) injected with Gd^{3+} loaded PMAA−PS 80-g-St nanoparticles (0.05 mmol/kg Gd^{3+}) at baseline (left column) and 30 min post-injection (center column). An anatomical map is presented in the right column. (B) Longitudinal relaxation rates (R_1) of sagittal sinus, ventricles, cortex, and subcortex for Gd^{3+} loaded PMAA−PS 80-g-St-DTPA polymer overtime. The bottom figure shows R_1 values for the different brain regions up to 180 min. The asterisk (*) denotes a significant difference ($p < 0.05$) in R_1 values compared to baseline.

Dox was omitted from these formulations to prevent possible confounding effects of Dox-induced BBB damage on the nanoparticle biodistribution. Similarly, the nanoparticle biodistribution was investigated in healthy Balb/c mice without brain tumors as previous studies have suggested that brain tumor-associated vasculature may be compromised and "leaky".[31]

MRI of Nanoparticle Distribution in Healthy Brain. Qualitative and quantitative information on nanoparticle brain distribution was inferred from MRI generated longitudinal relaxation rate R_1 ($1/T_1$) maps with the assumption that the change in R_1 relaxation rate, relative to the pre-scan, was dominated by the change in nanoparticle concentration. Examination of the R_1 map of the different brain slices at pre- and post-injection of nanoparticles revealed enhancement in certain brain areas such as sagittal sinus, ventricles, and to a lesser extent the cortex and subcortical areas (Figure 3A). At 30 min post-injection, the R_1 values were measured at 1.1 ± 0.1, 1.1 ± 0.1, 1.6 ± 0.2, and 1.7 ± 0.1 s^{-1} for cortex, subcortex, ventricles, and sagittal sinus, respectively (Figure 3B). These values decreased to 1 ± 0.1, 0.9 ± 0.1, 1.5 ± 0.3, and 1.1 ± 0.1 s^{-1} at 180 min post-injection. Values shown are the means and standard deviations for n = 3 independent experiments.

MRI offers the advantage of imaging brain parenchyma with high resolution and good contrast between different tissues, making this modality particularly useful for monitoring different regions or subregions of the brain. However, MRI is susceptible to motion and magnetic field inhomogeneity artifacts and has low inherent sensitivity limiting its application for detecting

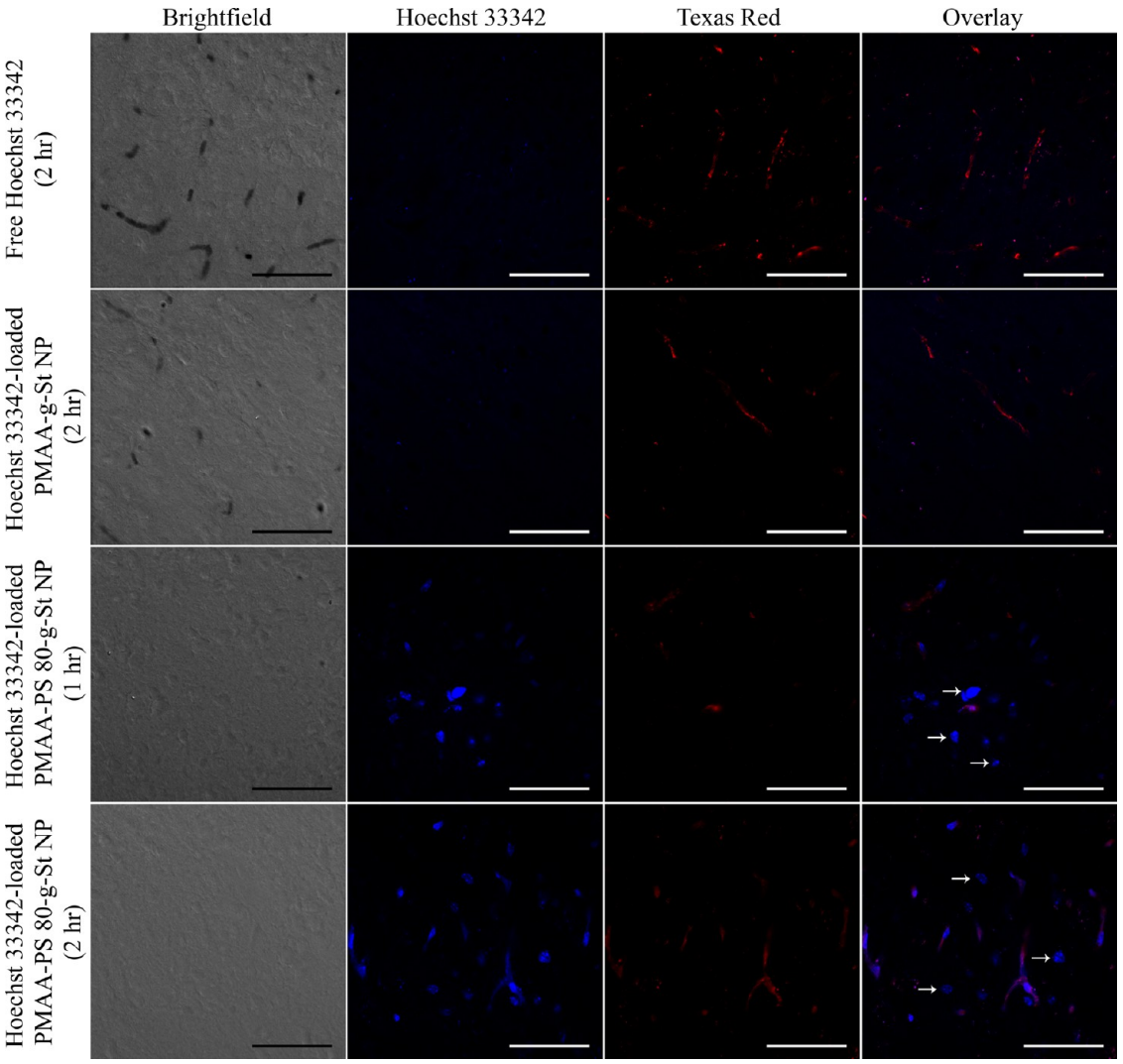

Figure 4. Laser scanning confocal microscopic images of healthy Balb/c mice sections following treatment with free Hoechst 33342, Hoechst 33342 loaded within PMAA-g-St NPs (without PS 80), or Hoechst 33342 loaded within PMAA−PS 80-g-St terpolymer NPs. Mice were treated for 1 or 2 h. Blood vessels were labeled by iv administration of Texas Red-dextran 15 min before euthanasia. Hoechst 33342 and Hoechst 33342-labeled cell nuclei appear blue. Texas Red-dextran appears as red. Arrows indicate representative Hoechst 33342 stained nuclei located away from blood vessels. Scale bar = 50 μm. Three-dimensional representation of the tissue sections are available in Figures S3−S6 (Supporting Information).

small quantities of nanoparticles in various brain regions.[41] For this reason, confocal laser scanning microscopy was used to investigate the ability of the nanoparticles to enter into the healthy mouse brain.

Delivery of BBB-Impermeable Dye into Healthy Brain. Nanoparticles with and without PS 80, loaded with a BBB-impermeable fluorescent dye (Hoechst 33342) that binds to nucleic acids were administered *via* intravenous (iv) tail vein injection to healthy Balb/c mice and allowed to circulate for up to 2 h. Laser scanning confocal microscopy was used to examine brain tissue sections in three dimensions for cell nuclei stained with Hoechst 33342 (blue) in relation to brain tissue structures including neuron bodies and brain vasculature (Figure 4). Brain vasculature was labeled with dextran conjugated with Texas Red fluorophore (red). Free Hoechst 33342, or loaded within PS 80-free nanoparticles, was unable to cross the BBB when administered iv and thus unable to stain cell nuclei in the brain (Figures 4 and S3−S6, Supporting Information). In contrast, Hoechst 33342 loaded within PMAA−PS 80-g-St nanoparticles was able to enter into the brain and label cell nuclei located away from brain capillaries. Co-localized nonspecific autofluorescence signal observed in both the Hoechst 33342 (blue) and Texas Red (red) filter sets are due to autofluorescing brain tissue components (*e.g.*, lipofuscin) which have broad emission spectra.[42]

These results indicate that PMAA−PS 80-g-St nanoparticles were able to enter the normal brain and further suggest that PS 80 might play a role in nanoparticle transport across the BBB to gain entry into the CNS. Indeed it has been suggested that coating nanoparticles with PS 80 leads to the enhanced adsorption

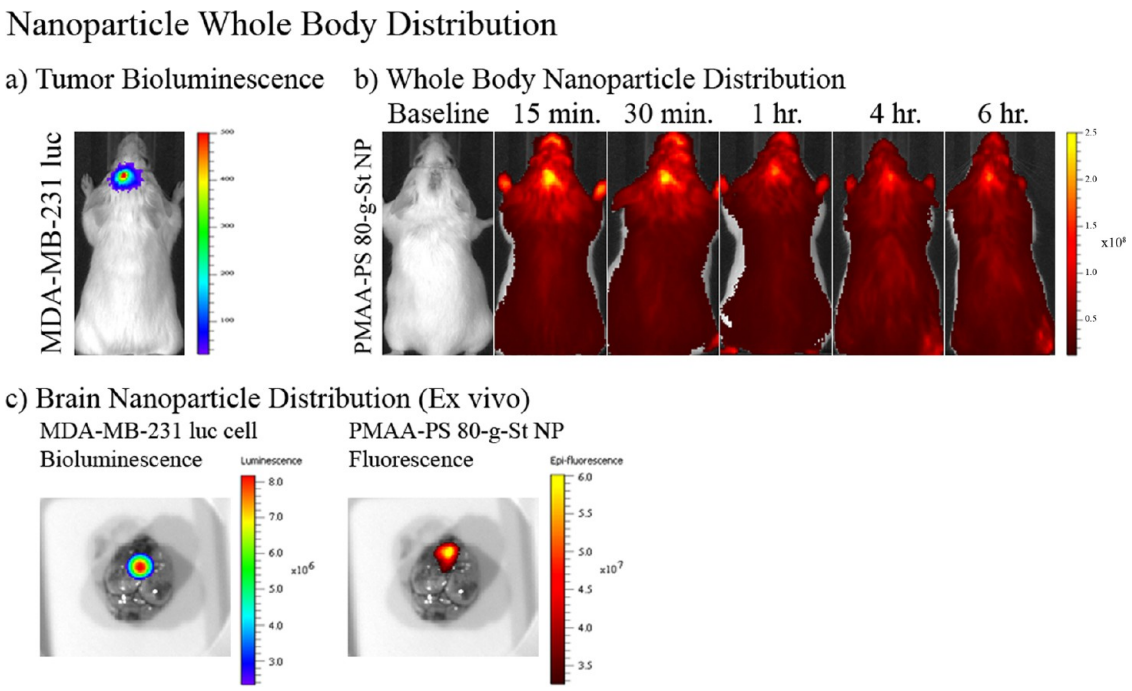

Figure 5. Brain tumor location and whole-body nanoparticle distribution. The brain metastasis of MDA-MB-231-luc-D3H2LN was established by intracranial injection. (a) Bioluminescence of luciferase expressing tumor cells 10 min following ip injection of luciferin solution. (b) PMAA−PS 80-g-St nanoparticles were labeled with a near-infrared dye (HiLyte Fluor 750) and imaged for up to 6 h after tail vein injection. (c) Bioluminescent image of brain tumor (left) and fluorescence image of nanoparticles (right) in an excised mouse brain.

of apolipoprotein-E (Apo-E) from the blood to the particle surface, and that the presence of Apo-E promotes nanoparticle internalization in the brain capillary endothelial cells *via* members of the LDL receptor family expressed by these cells.[26,27] Due to presence of PS 80 on the surface of PMAA−PS 80-g-St nanoparticles, as shown by our TOF-SIMS investigations (Figure 2), it is possible that a similar mechanism is also responsible for uptake of the terpolymer nanoparticles by the brain capillary endothelial cells.

Accumulation of Dox-Loaded PMAA−PS 80-g-St Nanoparticles in Breast Cancer Brain Metastases. *Breast Cancer Brain Metastasis Model.* Breast cancer metastases to the brain are most prevalent in the triple negative and HER2+ breast cancer subpopulations,[32,43,44] with the triple-negative subtype being particularly aggressive and unresponsive to targeted therapies due to lack of molecular target.[45,46] Therefore, we established a metastasis model using MDA-MB-231-luc-D3H2LN triple-negative human breast cancer cell line. These cells overexpress LDL receptors,[17,47] enabling LDL receptor-mediated cell uptake of the nanoparticles following transport across the BBB. This metastatic brain tumor model was developed in immunodeficient female SCID mice using stereotactic intracranial injection of ~50 000 MDA-MB-231-luc-D3H2LN human breast cancer cells into the primary somatosensory cortex.[48,49] Brain tumor growth was monitored *in vivo* by bioluminescence imaging (Figure 5a).

Tumor proliferation at the injection site and infiltration into the brain parenchyma was observed over a 2 week period following inoculation. At the injection site, metastatic foci formed along the direction of needle insertion along with neoplastic cell infiltration into brain parenchyma at sites such as the hippocampus. Small neovascular inclusions were also observed at this site between the Cornu Ammonis (CA) 1 and the dente gyrus. Numerous small independent metastatic foci were also observed distal to the injection site both within the cortex and the basal ganglia (data not shown). The stereotactic injection method is highly reproducible and exhibits a metastatic growth pattern similar that described by Saito *et al.*[48] The aggressive nature of brain metastasis using this breast cancer model is evident from the large number of tumor foci. This resembles breast cancer metastases in humans, which are difficult to treat by standard treatment options, *e.g.*, surgical resection. Normally, for patients with more than four lesions, surgery is not recommended.[50] Thus, this animal model is suitable for testing systemic chemotherapy.

In Vivo Nanoparticle Distribution in Tumor Bearing Mice. The tumor accumulation of HF 750-labeled terpolymer nanoparticles loaded with Dox was tracked in brain tumor-bearing mice for up to 6 h after intravenous injection in the tail vein using near-infrared fluorescence imaging (Figures 5b and S7, Supporting Information). The nanoparticles localized in the tumor region at 15 min post-injection and remained there for at least 6 h (Figure 5b). The *in vivo* finding was confirmed *ex vivo* in the dissected brain (Figure 5c) 6 h

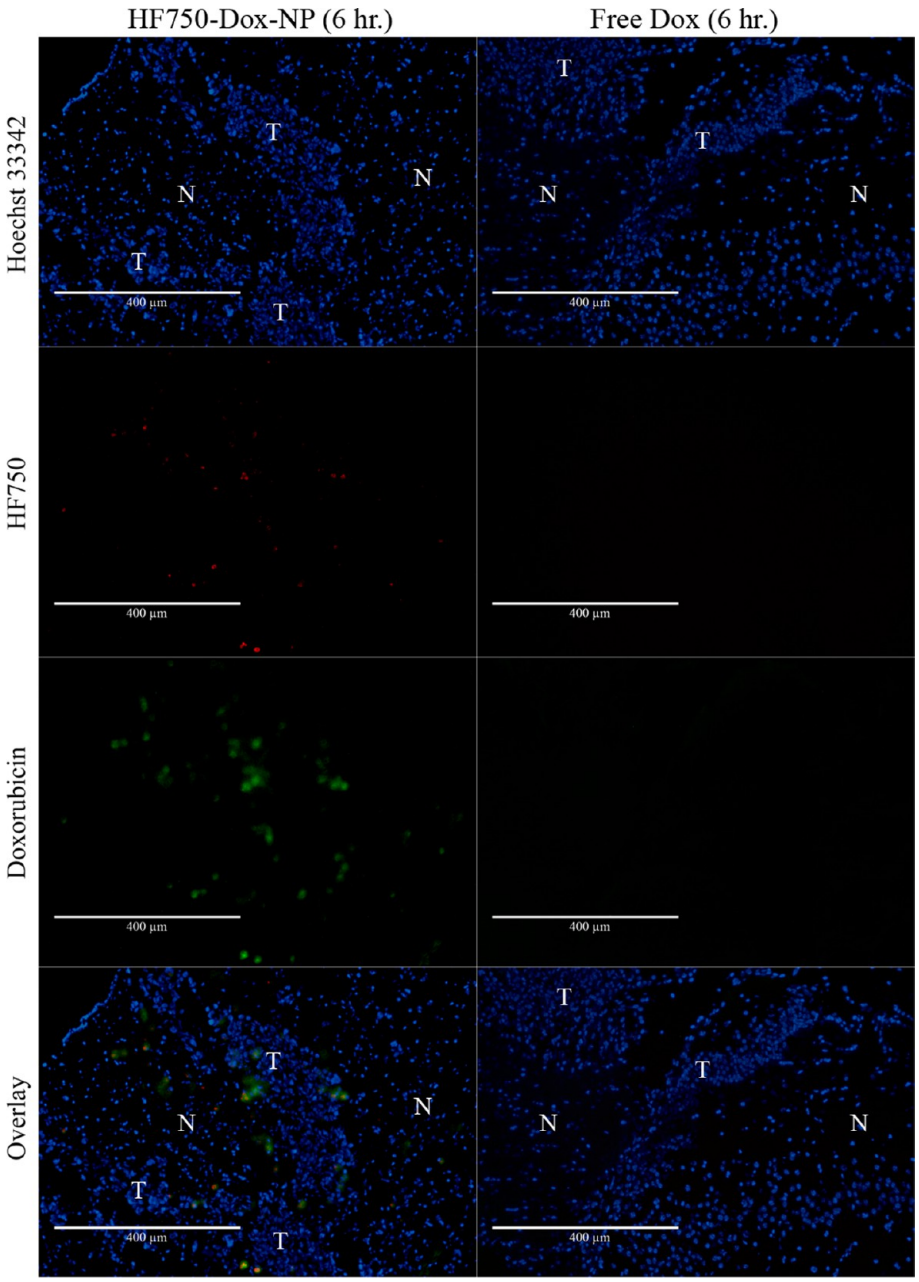

Figure 6. Fluorescence images of tumor-bearing mouse brain sections 6 h following intravenous injection of HF 750-labeled, Dox-loaded nanoparticles (left column) or free Dox (right column). Hoechst 33342-stained cell nuclei shown in blue, HF750-tagged nanoparticles shown in red, and Dox shown in green. A composite image shows the nanoparticle and Dox distribution around the brain tumor. Tumor identified as areas of hypercellularity (T) compared to normal tissue (N). Colocalization of the nanoparticles (red) and Dox (green) suggests that Dox is delivered by and released from the nanoparticles in the tumor-bearing brain.

post-injection, using the same imaging techniques. The colocalization of both tumor bioluminescence and nanoparticle fluorescence strongly suggests accumulation of nanoparticles in the brain tumor. The distribution of the nanoparticles in whole body was imaged at 15 min, 1 and 2 h by placing the mice on the back. Nanoparticle uptake in major organs such as the liver was examined *ex vivo* at 2 h post-injection. The results are presented in Figure S7 (Supporting Information). Both *in vivo* and *ex vivo* images indicate that uptake of the nanoparticles by the liver is insignificant; there is even less uptake in the spleen. The relatively stronger fluorescence intensity in the gallbladder and the kidneys at 2 h suggest the nanoparticles are likely eliminated by the biliary and renal pathways.

Microdistribution of Nanoparticle in Tumor Bearing Brain Tissue. Histological analysis of tumor-bearing brain tissue sections from mice treated with Dox-loaded nanoparticles or free Dox as a comparator was performed to examine the microscopic distribution of the nanoparticles and Dox. Fluorescence

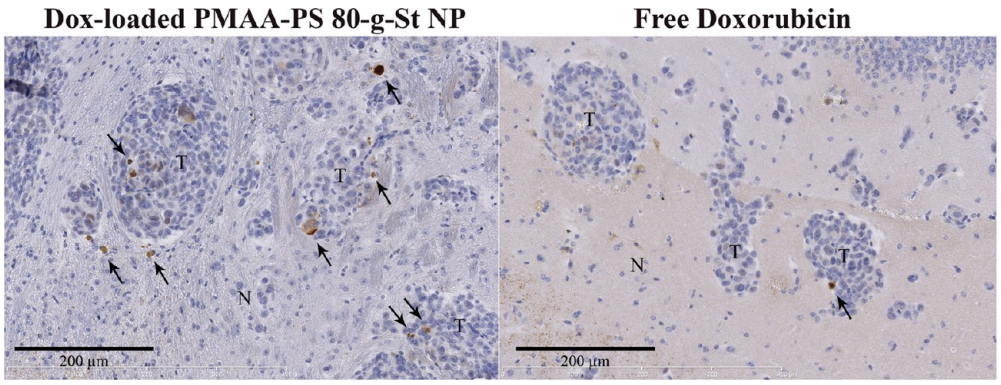

Figure 7. Cells expressing activated caspase-3 in metastatic brain tumors. Tumor-bearing brain sections prepared from mice 24 h following intravenous injection of HF 750-labeled, Dox-loaded nanoparticles (left) or free Dox (right). Tumor tissue denoted by marked hypercellularity (T). Normal brain tissue (N). Caspase-3-(+) cells shown in brown (arrows).

TABLE 2. Number of TUNEL-(+) and Activated Caspase-3 Expressing Cells/mm^2 of Tumor Area[a]

	no. activated caspase-3 expressing cells (per mm^2)	no. TUNEL-(+) cells (per mm^2)
Dox PMAA−PS 80-g-St NPs (n = 4)	10.5 ± 1.7	43.4 ± 9.6
Free Dox (n = 3)	1.7 ± 0.6	2.9 ± 6.0
p-value (p)	<0.001	<0.0001

[a] Cell counts presented as average ± SD; n > 3.

images were acquired using the appropriate filter sets to visualize NIR HF 750-labeled nanoparticles, Dox, and Hoechst 33342 stained nuclei, respectively. Brain tumor tissue was identified by areas of hypercellularity as evident from Hoechst 33342 stained cell nuclei shown in blue in Figure 6. Mice treated with the Dox-loaded nanoparticle formulation demonstrated nanoparticle and Dox accumulation along the brain tumor periphery (Figure 6). Colocalization of nanoparticles (red) with Dox (green) around the tumor suggests that the nanoparticle delivered Dox to the tumor site and released Dox there. Marked nanoparticle and Dox accumulation around the large tumors may be due to a combination of both LDLR-mediated nanoparticle transport across the BBB and the enhanced permeability and retention (EPR) effect.

In contrast, Dox was absent from the tumor site in mice treated with the free Dox formulation. This result is consistent with previous findings demonstrating the inability of free Dox to penetrate the BBB.[51] Apparently, the administration of Dox-encapsulated PMAA−PS 80-g-St nanoparticles enabled higher Dox concentrations in the brain tumor at 6 h post treatment compared to free Dox.

Doxorubicin Loaded PMAA−PS 80-g-St Nanoparticles Inhibit Tumor Growth. *Doxorubicin Loaded PMAA−PS 80-g-St Nanoparticles Selectively Induced Cancer Cell Apoptosis.* Brain sections prepared from tumor-bearing SCID mice treated with free Dox or Dox-loaded nanoparticles (10 mg of Dox per kg of mouse bodyweight, administered iv) were stained for cleaved caspase-3 and TUNEL nick-end labeling 24 h post treatment to examine cancer cell apoptosis as an early indication of drug efficacy. Tumors are identified as regions of marked hypercellularity and decreased ground substance with distinct tumor margins in TUNEL-stained sections. Caspases exist as inactive proenzymes in the normal cell which, once activated in the presence of apoptotic stimuli, plays a central role in the initiation and propagation of programmed cell death.[52] Caspase-3 is responsible for chromatin condensation and DNA fragmentation, and is an early marker of cell apoptosis. The TUNEL reaction is a commonly used method for detecting fragmented DNA that results from apoptotic signaling cascades and is an indicator of late-stage apoptosis.

A marked number of cells expressing activated caspase-3 can be found within and surrounding tumor micrometastases in mice treated with Dox loaded nanoparticles (Figure 7, Table 2). Such staining of activated caspase-3 is not observed in free Dox-treated mice, indicating that the nanoparticle formulation of Dox is able to induce higher cell apoptosis compared to the free drug 24 h following treatment. Similarly, a greater number of TUNEL-(+) apoptotic cells were found distributed throughout large metastatic brain tumors (Figure 8, Table 2) and adjacent to micrometastases (Figure 9, Table 2) of mouse brain treated with Dox loaded nanoparticles compared to free-Dox treatment. In Figures 8 and 9, tumor foci can be identified as areas of hypercellularity and by areas of low background compared to the healthy brain tissue. The difference in background fluorescence signal is attributed to autofluorescence of the tissue ground substance in

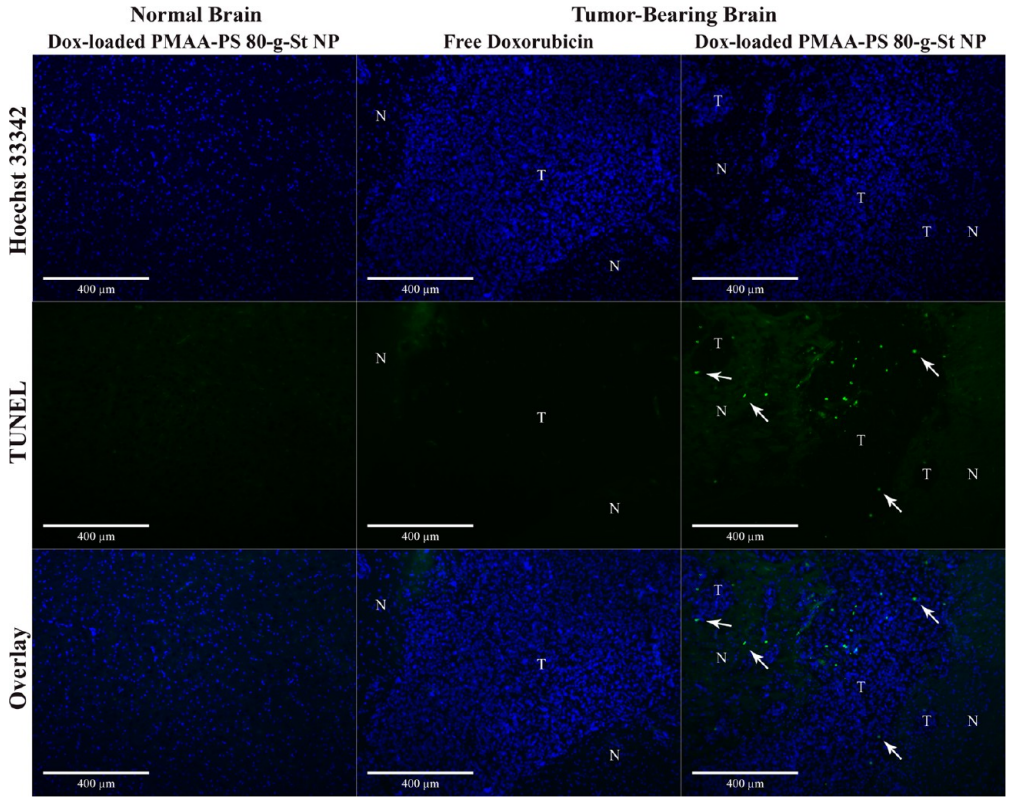

Figure 8. TUNEL assay for apoptosis in large brain tumors. Tumor-bearing brain sections prepared from mice 24 h following intravenous injection of HF 750-labeled, Dox-loaded nanoparticles in normal brain (left column), free Dox (center column), or Dox loaded nanoparticles (right column). First row: Hoechst 33342-stained cell nuclei shown in blue. Tumor tissue denoted by marked hypercellularity (T). Normal brain tissue (N). Second row: FITC-labeled TUNEL-(+) cells shown in green (arrows). Tumor tissue denoted in dark green due to absence of ground substance. Third row: A composite image showing TUNEL-(+) cells in relation to tumor tissue.

the normal brain, and absence of this ground substance within the tumors. Importantly cell apoptosis is not observed in normal brain tissue (Figure 8, left panel). These results suggest that administration of Dox loaded nanoparticles to tumor-bearing mice is able to induce tumor-specific apoptosis around both large brain tumors and micrometastases within 24 h of treatment. Induction of tumor cell apoptosis may be attributed to the delivery of Dox rather than the nanocarrier itself as the PMAA-Ps 80-g-St terpolymer NPs were reported nontoxic in several cell lines[36] and found to be nontoxic to MDA-MB-231-luc cells at concentrations as high as 500 μM as determined by the MTT assay (Figure S8, Supporting Information).

The observed specific cytotoxicity of the Dox loaded nanoparticles in cancer cells in the brain may stem from (1) the capability of the terpolymer nanoparticles entering the brain and targeting the metastasis lesions (first-stage targeting *via* LDLR-mediated mechanism and EPR effect), (2) the specificity of binding to MDA-MB-231 cancer cells as a function of LDLR expression following the BBB-permeation (second-stage targeting), and (3) the mechanism of Dox, which induces apoptosis through interference with DNA repair and elevations in ceramide production, preferentially impends the replication of highly proliferative cells (*e.g.*, metastatic cancer) through DNA intercalation, while exhibiting few effects on nonreplicating cell populations such as neurons.[52]

In larger brain metastasis lesions (*e.g.*, larger than 0.25 mm in diameter), the BBB and efflux pump expression may be compromised,[53,54] allowing systemically delivered therapeutic agent to reach the tumor site and illicit a response to some degree. This disruption of the BBB is less significant in smaller micrometastases (*e.g.*, smaller than 0.25 mm), preventing drug from reaching the cancer cells.[31] While chemotherapy of large primary lesions in the brain have been reported in the past,[25,55] the ability of the nanocarrier system to induce apoptosis within micrometastases in the brain is very important because drug penetration to micrometastases is much more difficult where the blood vessels are intact. Hence, drug delivery *via* nanoparticle transcytosis across the undisrupted BBB is critical.

Doxorubicin Loaded PMAA−PS 80-g-St Nanoparticles Inhibit Brain Tumor Growth. To evaluate the effect of Dox-loaded NPs on tumor growth inhibition, a brain metastasis model was established in immunodeficient female NRG-SCID mice by stereotactic intracranial injection of ~100 000 MDA-MB-231-luc D3H2LN human

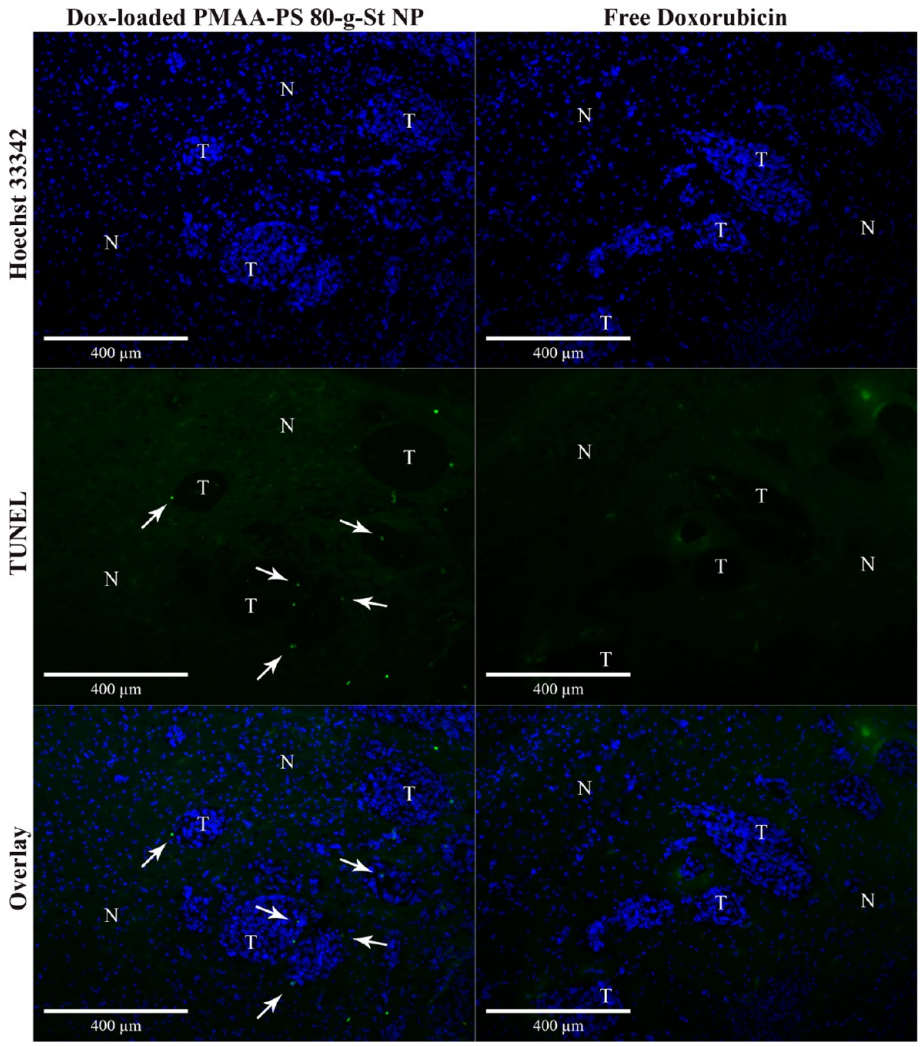

Figure 9. TUNEL assay for apoptosis around brain tumor micrometastases. Tumor-bearing brain sections prepared from mice 24 h following intravenous injection of HF 750-labeled, Dox-loaded nanoparticles (left column) or free Dox (right column). First row: Hoechst 33342-stained cell nuclei shown in blue. Tumor tissue denoted by marked hypercellularity (T). Normal brain tissue (N). Second row: FITC-labeled TUNEL-(+) cells shown in green (arrow). Tumor tissue denoted in dark green due to absence of ground substance. Third row: A composite image showing TUNEL-(+) cells in relation to tumor tissue.

triple negative breast cancer cells into the cortex (Figure 10). NRG-SCID mice were selected for these experiments because they can tolerate higher doses of Dox required for therapeutic effect compared to SCID mice which lack some mechanisms of DNA repair. At 2 and 4 weeks following tumor inoculation, the mice were treated with free Dox, Dox-loaded PS 80-containing NPs (10 mg Dox per kg mouse body weight, 200 μL administered iv), or saline (200 μL) as a control. Tumor growth was monitored *in vivo* using bioluminescence imaging.

Brain tumor bearing mice treated with saline or free Dox exhibited rapid tumor growth following tumor inoculation (Figure 10). The ineffectiveness of free Dox is in agreement with previous observations as Dox is unable to penetrate through the BBB at appreciable levels.[7] In contrast, brain tumor treated with Dox-loaded PMAA−PS 80-g-St NPs underwent a much slower growth rate indicated by the significantly lower bioluminescence signals. At days 14, 21 and 28, the tumor inhibition rates of Dox-loaded PMAA−PS 80-g-St NPs relative to free Dox are 3.4, 11.7, and 8.8 fold, respectively. These results suggest that PMAA−PS 80-*g*-St NPs are able to deliver Dox across the BBB to intracranial lesions of triple negative breast cancer and inhibit tumor growth.

Note that we did not observe a statistically significant correlation between tumor size and mouse body weight. That is to say that some mice with relatively small tumors experienced significant weight loss while others with relatively large tumors experienced minimal weight loss. This may be a result of the aggressive metastatic nature of the MDA-MB-231-luc D3H2LN breast cancer brain tumor model and the fact that specific locations within the brain are more critical to body weight loss than others. A small metastatic lesion located at a critical region within the brain may be more detrimental to animal health than a large lesion

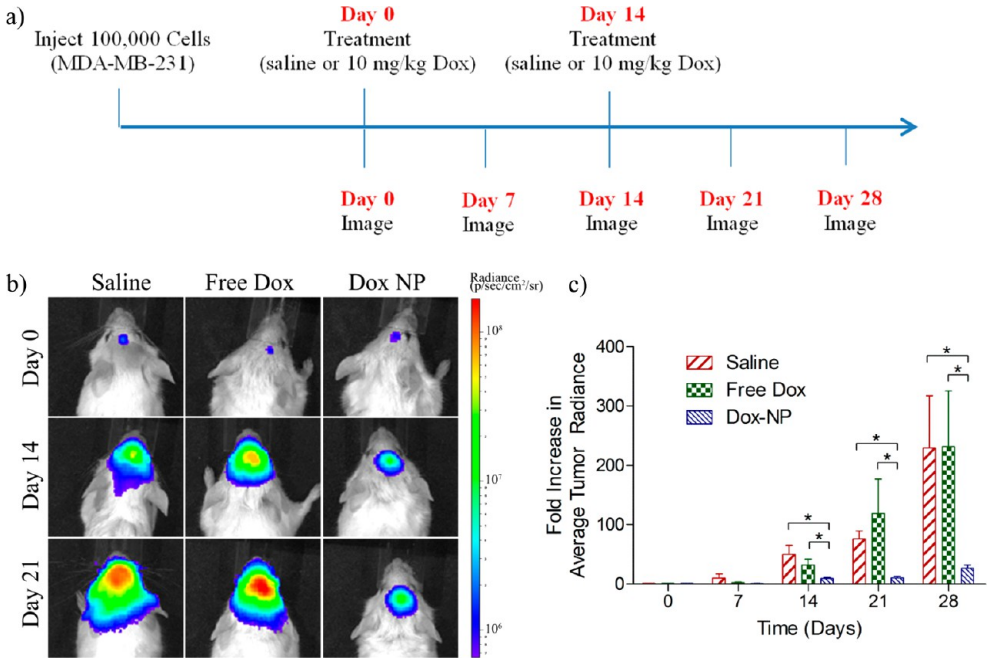

Figure 10. Brain tumor growth inhibition in NRG-SCID mice. (a) Treatment schedule with saline (200 μL), Dox (10 mg/kg; 200 μL), or Dox-loaded NPs (10 mg/kg Dox; 200 μL). Treatments were administered on day 0 and 14. (b) *In vivo* images of brain tumor bioluminescence. (c) Fold increase in the average tumor radiance as measured by *in vivo* bioluminescence imaging. Data presented as mean $\pm$ SEM (n = 5 for saline; $n \geq 7$ for free Dox and Dox-NP). Statistical significance of $p < 0.05$ denoted by asterisk (*).

elsewhere. Thus, the health and survival of metastatic brain tumor bearing mice may be highly dependent on tumor location rather than size.

CONCLUSIONS

A multifunctional nanotheranostic system based on PMAA–PS 80-g-St terpolymer for the delivery of anticancer drug and imaging agents to the brain and brain metastases of breast cancer is presented. The ability of the nanocarrier to enter the brain and extravasate from intact brain microvessels of healthy mice was demonstrated by *in vivo* MRI and *ex vivo* confocal microscopy. The Dox-loaded nanoparticles accumulated in the intracranial breast cancer brain metastases quickly and released Dox in the metastatic lesions, as detected by histological analysis and fluorescence microscopy, whereas no Dox was detectable in the samples treated with free Dox. A large number of apoptotic cells were detected in both large metastatic lesions and micrometastases 24 h following treatment with Dox-loaded nanoparticles, while few were detected in the normal brain tissue, indicating cancer-cell specific cytotoxicity of the treatment. In contrast, few apoptotic cells were observed in the free-Dox control. Treatment with Dox-loaded nanoparticles reduced brain tumor growth in NRG-SCID mice compared to free Dox. These results suggest that PMAA–PS 80-g-St nanoparticles are a promising theranostic system for the delivery of drugs and contrast agents to the brain and for the treatment of brain metastases of breast cancer.

METHODS

Soluble corn starch (MW = 11 000 g/mol), methacrylic acid (MAA), sodium thiosulfate (STS), potassium persulfate (KPS), polysorbate 80 (PS 80), sodium dodecyl sulfate (SDS), fluoresceinamine isomer I (FA), *N*-(3-(dimethylamino)propyl)-*N*′-ethylcarbodiimide hydrochloride (EDC), *N*-hydroxysuccinimide (NHS), gadolinium chloride hexahydrate (Gd), diethylenetriaminepenta acetic acid (DTPA), and all other chemicals unless otherwise mentioned were purchased from Sigma-Aldrich Canada (Oakville, ON, Canada). HiLyte Fluor 750 hydrazide (HF 750) was purchased from AnaSpec (Fremont, CA). DTPA bis-anhydride (DTPA-bis-An) was synthesized in-house using a previously described method.[34]

Synthesis and Preparation of PMAA-Ps 80-g-St Polymer and Nanoparticles. *Synthesis of PMAA–PS 80-g-St Polymer.* PMAA–PS 80-g-St polymer was synthesized using a method described previously[33] with the following feed composition: 1.55 g of starch, 1.55 g of MAA, 1.5 g of PS 80, 0.25 g of SDS, 0.12 g of KPS, 0.20 g of STS. All the chemicals were dissolved in doubly distilled deionized (DDI) water to make a final volume of 200 mL. Briefly, 1.55 g of starch was dissolved in 150 mL of distilled water by heating at 70 °C for 30 min. The solution was purged with N_2 for 30 min to remove any dissolved oxygen. Subsequently, 0.25 g of SDS, 1.5 g of PS 80, 0.12 g of KPS, and 0.25 g of STS were added to the starch solution while being stirred. After 10 min, the reaction was started by addition of 1.55 g of nitrogen purged MAA. Opalescence appeared after 5 min and the reaction was continued for 8 h at 70 °C to ensure complete grafting. The product was dialyzed (molecular weight cutoff 25 000 g/mol) extensively against warm water for 3 days, against methanol for another 2 days and against water again for another 2 days. The purified polymer was then dried at 50 °C for 24 h, and stored in a desiccator for future use.

Preparation of GD^{3+} Loaded PMAA–PS 80-g-St Polymer. Gd^{3+} was loaded into the polymer using a method described previously.[34] Briefly, DTPA was conjugated to the starch terpolymer by addition of 1.5 g of DTPA-bis-anhydride to 3 g terpolymer dissolved in 50 mL of dry dimethyl sulfoxide (DMSO). The solution was stirred at room temperature for 24 h, dialyzed against DMSO for 48 h, and subsequently dialyzed against water for another 48 h. Loading of Gd^{3+} was achieved by dispersing the PMAA–PS 80-g-St-DTPA polymer (0.5 g) in 10 mL of distilled deionized water. The pH was adjusted to 6.5 using 0.1 N NaOH. Ten milliliters of aqueous solution of gadolinium chloride hexahydrate (10 mg/mL) was then added dropwise while stirring, and the pH of the reaction was kept at 6.5 with the 0.1 N NaOH. After stirring for 1 h, the product was dialyzed exhaustively against 0.9% NaCl until no free Gd^{3+} was detected in the wash medium using the xylenol orange test. The product was then neutralized and freeze-dried.

Preparation of Dye Loaded PMAA–PS 80-g-St Polymer. Covalent linkage of two fluorescence moieties, namely, HiLyte Fluor 750 (HF 750; λ_{ex} = 745 nm, λ_{em} = 820 nm) (0.4 mg) and FA (λ_{ex} = 496, λ_{em} = 520) (0.5 mg), to the polymer (40 mg) was achieved using a method previously described.[35] Briefly, to 2 mL of aqueous solution of purified polymer, 30 mg of EDC, and 30 mg NHS were added. After 30 min, 0.4 mg of HF 750 (1.25 mg/mL in DDI water) and/or 0.5 mg of FA was added under stirring. The mixture was protected from light and stirred at room temperature for 24 h. Finally, the product was neutralized to pH 7.5 using 0.1 N NaOH and purified by extensive dialyzing against DDI water.

Preparation of Hoechst 33342-Loaded PMAA–PS 80-g-St Nanoparticles. Hoechst 33342-loaded PMAA–PS 80-g-St nanoparticles were prepared by heating 250 μL of 10 mg/mL Hoechst 33342 solution, 100 μL of 40 mg/mL terpolymer solution, 100 μL of 100 mg/mL PF 68 solution, and 12 mg of ethyl arachidate to 65 °C. The mixture was stirred for 20 min. Nanoparticles were formed under ultrasonication using a Hielscher UP100H probe ultrasonicator, (Hielscher USA, Inc., Ringwood NJ, USA) for 10 min and suspended in sterile 5% dextrose to a final Hoechst 33342 concentration of 2.5 mg/mL. An analogous control formulation was prepared from PMAA-g-St-lipid polymer without PS 80.

Preparation of Self-Assembled Dox-Loaded PMAA–PS 80-g-St Nanoparticles. Self-assembled nanoparticles were prepared by first dissolving 8 mg of PMAA–PS 80-g-St polymer in 1.8 mL of sterile 5% dextrose. The polymer solution was then placed in an ice bath and, while under ultrasonication using a Hielscher UP100H probe ultrasonicator (Hielscher USA, Inc., Ringwood, NJ), 200 μL of Dox solution (12 mg/mL in 5% dextrose) was added in small increments to the polymer solution every 30 s. Ultrasonication continued for an additional 10 min. Addition of the Dox resulted in spontaneous formation of nanoparticles. The nanoparticles were then passed through ion exchange resins, Sephadex G50 fine (GE Healthcare, Piscataway, NJ) to remove unbound Dox.

Physicochemical Characterization of the PMAA–PS 80-g-St Polymer and Nanoparticles. ^{1}H NMR measurements for PMAA–PS 80-g-St polymer (15 mg/mL in 0.01 M NaOD solution) were obtained using a Varian Mercury 400 MHz spectrometer (Palo Alto, CA). The spectra were obtained over 64 scans using a pulse angle of 25°, a 2 s acquisition time, and a 10 s delay time. All chemical shifts are reported in parts per million (ppm) with the water peak as reference.

The particle size and the ξ-potential of the PMAA–PS 80-g-St nanoparticles were determined with Malvern Zetasizer Nano ZS (Worcestershire, U.K.). For size measurements, the particles were dispersed in pH of 7.4 phosphate buffered saline (PBS) with an ionic strength of 150 mM. For ξ-potential measurements, PBS buffers of pH 7.4 and ionic strength of 10 mM were used. The morphology of the nanoparticles was examined by transmission electron microscopy (TEM). TEM photographs were acquired on a Hitachi H7000 electron microscope (Mississauga, ON, Canada) with an accelerating voltage of 100 kV.

Time-of-Flight-Secondary Ion Mass Spectrometry. TOF-SIMS analysis was carried out on an ION-TOF TOFSIMS IV spectrometer (Munster, Germany). Analysis was performed with a 25 keV Ga^+ primary ion source. Negative secondary ions passing through a reflectron mass spectrometer (Agilent, Santa Clara, CA) were detected with a microchannel plate assembly operating at 10 kV post acceleration. The analysis area was 500 × 500 μm^2 to reduce charging effects.

Animal Models. All animal handling and procedures were conducted under an approved protocol from the Animal Care committee at the Ontario Cancer Institute following guidelines set forth by the Canadian Council on Animal Care (CCAC). Eight to 10 week old Balb/c mice (Jackson Laboratories, Bar Harbor, ME) were used to evaluate whole-body nanoparticle biodistribution and kinetics in normal (nontumor bearing) mice. Mice were fed water and food ad libitum, housed with a 12/12 h light/dark schedule in a temperature and humidity controlled room.

A brain metastatic breast cancer model was established in four to six week old SCID mice (Ontario Cancer Institute, Toronto, Canada) to evaluate nanoparticle and Dox brain tumor accumulation and subsequent tumor cell apoptosis. Luciferase-transfected human breast cancer cells (MDA-MB-231-luc-D3H2LN, obtained from Caliper Life Sciences and checked for mycoplasma contamination) 5×10^4/mouse were injected intracranially in a 2 μL volume into the cortex (about 3 mm depth) by using a stereotactic device. Tumors were monitored for growth with luciferine-induced (15 mg/kg, 10 min post intraperitoneal injection) bioluminescence imaging over the course of the two-week growth period using an Xenogen IVIS spectrum imager (Caliper Life Sciences, Inc., Hopkinton, MA).

A brain metastatic breast cancer model was established in four to six week old NRG-SCID mice (Ontario Cancer Institute, Toronto, Canada) to evaluate inhibition of brain tumor growth following treatment with Dox-loaded NPs, free Dox, or saline. Luciferase-transfected human breast cancer cells (MDA-MB-231-luc-D3H2LN, obtained from Caliper Life Sciences and checked for mycoplasma contamination) at 1×10^5/mouse were injected intracranially in a 2 μL volume into the cortex (about 3 mm depth) using a stereotactic device. Tumors were monitored for growth with luciferine-induced (15 mg/kg, 10 min post intraperitoneal injection) bioluminescence imaging over the course of the two-week growth period using an Xenogen IVIS spectrum imager (Caliper Life Sciences, Inc., Hopkinton, MA).

***In Vivo* Magnetic Resonance Imaging (MRI).** *In vivo* MRI used a 7 T micro-MRI spectrometer (BioSpec USR, Bruker, Ettlingen, DE), fitted with the B-GA12 gradient coil and a 7.2 mm inner diameter quadrature radiofrequency (RF) coil. Mice were anesthetized by breathing 1.8% isoflurane, and imaged in supine position on a custom slider bed. A 7.2 cm inner diameter linearly polarized cylindrical volume coil was used for RF transmission, and a dedicated murine brain receive-only RF coil was used for MR signal reception. A pneumatic pillow under the thorax/abdomen provided a signal for both physiologic monitoring and respiratory gated imaging (SA Instruments, Stony Brook, NY). Mice were also prepared *via* tail vein cannulation with a 27 G needle and a precision line (80 μL internal volume), to enable manual contrast injection following baseline scanning. Brain T_1 changes from baseline following contrast agent injection were measured using a respiratory-gated variable-flip-angle (VFA) approach. At each time-point, 3D-FLASH images were acquired sequentially in a vertical plane at flip angles of 2, 10, 20, and 30°, with all other data acquisition parameters held constant (Echo time (TE)/Repetition time (TR) = 2.6/25 ms, 128 × 128 × 16 matrix over a 16 × 16 × 16 mm field-of-view providing 0.125 × 0.125 × 1 mm spatial resolution, 81.5 kHz readout bandwidth). The acquisition time for each flip angle was approximately 2 min. R_1 maps were generated from signal and flip angle data pairs following linearization of the MR signal equation by linear regression (Matlab, The Mathworks, Natick, MA). Quantitative measurements were performed in manually segmented cortical, subcortical, and sagittal sinus subregions, which were registered across all time-points, using MIPAV software (National Institutes of Health, Bethesda, MD). Matching multislice T_2-weighted 2D-RARE (Rapid acquisition relaxation enhancement) images with RARE factor of 16 were also acquired using the following data acquisition parameters: TE = 72 ms, TR = 4400 ms, readout bandwidth = 50 kHz, scan time = 4 min 24 s,

FOV = 100 × 100-μm over 16 × 16 mm, and slice thickness of 1 mm (16 slides).

***In Vivo* Whole-Body Fluorescence Imaging.** Whole-body *in vivo* nanoparticle biodistribution and tumor accumulation in healthy Balb/c and tumor-bearing SCID mouse brain was examined using Xenogen IVIS spectrum imager (Caliper Life Sciences, Inc., Hopkinton, MA) at 745 nm excitation and 820 nm emission wavelengths. Mice were anesthetized with 1.8% isoflurane prior to whole-body *in vivo* imaging.

***Ex Vivo* Fluorescence Imaging of the Brain.** To examine nanoparticle accumulation in brain tumor-bearing SCID mice, fluorescently labeled nanoparticles (200 μL injection volume; 8 mg/mL polymer; 10 mg/kg Dox for tumor-bearing mice) were injected into the lateral tail vein of the mice. At predetermined time points, the mice were euthanized by CO_2 asphyxiation, and the brain was dissected. NIR fluorescence images of the dissected brains were obtained using the Xenogen IVIS spectrum imager (Caliper Life Sciences, Inc., Hopkinton, MA). The brain fluorescence intensities were then quantified by drawing the region of interest (ROI) using the analysis software package supplied by the manufacturer. The accumulation of the nanoparticles in the brain was evaluated by measuring the ratio of NIR fluorescence intensity of nanoparticle injected tissue to untreated tissue.

Delivery of BBB-Impermeable Dye into Healthy Brain. To examine nanoparticle penetration into healthy brain, Balb/c mice were treated with 200 μL of Hoechst 33342-loaded nanoparticles with PS 80 (PMAA−PS 80-g-St) or without PS 80 (PMAA-g-St) (2.5 mg/mL dye), or free Hoechst 33342 (2.5 mg/mL in saline) *via* tail vein injection. Mice were euthanized 1 or 2 h following treatment. Texas red-labeled dextran (10 000 MW, Life Technologies, CA) was administered intravenously 15 min prior to euthanasia. The brain was dissected, fixed in 10% formalin for 3 h, transferred to 30% dextrose solution overnight, embedded in Tissue-Tek OCT resin (Somagen, Torrance, CA) and finally flash frozen. Thaw mounted 20 μm thick frozen sections were obtained on a Leica, model CM3050S cryostat and analyzed using Zeiss LSM700 confocal microscope and fluorescent excitation and emission filters appropriate for detection of the indicated chromophores within the cortex (Dextran, Texas Red, Ex./Em. = 595/615 nm; Hoechst 33342, Ex./Em. = 352/461 nm).

Nanoparticle Microdistribution Tumor-Bearing Brain Tissue. To investigate nanoparticle accumulation and Dox release in tumor-bearing brain tissue, HF 750-labeled nanoparticles (200 μL injection volume; 8 mg/mL polymer; NPs were loaded with 10 mg Dox per kg mouse bodyweight) were injected into the tail vein of metastatic breast cancer brain tumor-bearing SCID mice. Six hours post treatment, the mice were euthanized and the brain tissues were dissected, frozen, and sliced into 10 μm thick sections. The air-dried samples were imaged using an AMG EVOS FL fluorescence microscope (Thermo Fisher Scientific, Inc., Waltham, MA). Nanoparticle distribution around the tumor was examined within the QD800 emission window (Ex/Em. = 710/800 nm). Doxorubicin localization was imaged over the GFP spectral window (Ex./Em. = 470/525 nm). Cell nuclei were imaged within the DAPI spectral window (Ex./Em. = 344−357/447−460 nm) after incubation with Hoechst 33342 trihydrochloride, trihydrate (Invitrogen, 1:10 000 dilution) and rinsing with PBS (pH 7.4). Photo contrast corrections and overlays were performed using Adobe Photoshop software.

Apoptosis in Tumor-Bearing Brain Tissue. To investigate brain tumor cell apoptosis following Dox-loaded NP or free Dox treatment, 200 μL of PMAA−PS 80-g-St nanoparticles (8 mg/mL polymer; NPs were loaded with 10 mg of Dox per kg mouse bodyweight), or free Dox (10 mg/kg), was administered *via* lateral tail vein injection into metastatic breast cancer brain tumor-bearing SCID mice. The mice were euthanized 24 h following treatment. The brain samples were bisected along their midline and postfixed in 4% paraformaldehyde, 0.1 M PBS overnight at 4 °C. Specimens were then removed from fixation, flushed, and equilibrated in 30% sucrose at 4 °C, embedded in Tissue-Tek OCT resin (Somagen, Torrance, CA) and finally flash-frozen. Thaw mounted 10 μm thick frozen sections were obtained on a Leica, model CM3050S cryostat (Concord, ON, Canada). Tumor cell apoptosis was determined by TUNEL reaction (TdT *In Situ* Apoptosis Detection Kit, R&D Systems, Minneapolis, MN) and immunofluorescent labeling of cleaved caspase-3. The TUNEL reaction product was visualized with streptavidin−biotin-FITC complex at 10× magnification. Apoptotic TUNEL-(+) and caspase-3-(+) cells were imaged using a Nikon Eclipse E1000 motorized microscope equipped with a 270° rotating stage, Nomarski contrast optics, and fluorescent excitation and emission filters appropriate for detection of the indicated chromophores (DAPI, Ex./Em. 358/461 nm; FITC, Ex./Em. 470/525 nm) (Tokyo, Japan). Images were captured using a Hamamatsu C4742-95 camera (Hamamatsu, SZK, Japan). Measurement of TUNEL-(+) and caspase-3-(+) cells was performed on >2 visual fields per brain. The number of apoptotic cells within each field was normalized to the tumor area, and this was averaged for each animal for statistical analysis. The number of apoptotic cells for each treatment was taken as the average of the animal normalized apoptotic cell numbers.

Tumor Growth Inhibition Study. Tumor bearing NRG-SCID mice were used to evaluate tumor growth inhibition. Luciferase-trasfected human breast cancer cells (MDA-MB-231-luc-D3H2LN) were injected intracranially into the cortex. The first treatment with free Dox, Dox-loaded NPs (10 mg Dox per kg mouse body weight, 200 μL administered iv), or saline (200 μL) was administered on day 0, between 1 and 2 weeks following inoculation depending on the tumor size as measured through *in vivo* bioluminescence imaging. A second treatment was administered 2 weeks later on day 14. Tumor growth was monitored *in vivo* using bioluminescence imaging for up to 4 weeks following the first treatment. The fold increase in average tumor size was obtained by normalizing the tumor radiance over the course of the experiment to the initial tumor radiance at day zero.

Statistics. A commercial statistical software package (SPSS version 13.0, SPSS Institute, Chicago, IL) was used for statistical analysis. Data was presented as a means ± standard deviation (SD and/or SEM), and analyzed using the Student's *t*-test. $P < 0.05$ was considered statistically significant, and all probabilities were two-tailed.

Conflict of Interest: The authors declare no competing financial interest.

Supporting Information Available: Further experimental details regarding the NMR characterization of the PMAA-PS 80-g-St polymer structure, TEM images of the terpolymer nanoparticles, laser scanning microscopy images of Hoechst 33342 delivery to healthy brain, fluorescent imaging of *in vivo* whole body biodistribution and organ uptake, *in vitro* nanoparticle cytotoxicity of MDA-MB-231-luc cells to nanoparticles and free Dox, and NP delivery of Hoechst to brain (avi). This material is available free of charge *via* the Internet at http://pubs.acs.org.

Acknowledgment. The authors gratefully thank the Natural Sciences and Engineering Research Council (NSERC) of Canada for the Discovery Grant and the Equipment Grant to X. Y. Wu that enabled exploration of the new polymer system, the Canadian Institutes of Health Research (CIHR) for the operating grant to X. Y. Wu and A. M. Rauth that supported the *in vivo* evaluation of the polymer system for delivering anticancer drug and imaging agents to the brain metastases. The scholarships from the Natural Sciences and Engineering Research Council (NSERC) of Canada to J. Li, Ontario Graduate Scholarship to P. Prasad and J. Li, University of Toronto fellowships and Ben Cohen scholarships to J. Li, P. Prasad and A. Shalviri are also sincerely acknowledged. The authors would also like to acknowledge the Spatio-Temporal Targeting and Amplification of Radiation Response (STTARR) program and its affiliated funding agencies. The authors also acknowledge C. D. Soeandy for her assistance in preparing histology sections, and Lily Morikawa at the Pathology Core of the Centre for Modeling Human Disease, at The Lunefeld-Tanenbaum Research Institute.

REFERENCES AND NOTES

1. Norden, A. D.; Wen, P. Y.; Kesari, S. Brain Metastases. *Curr. Opin. Neurol.* **2005**, *18*, 654–661.
2. Fidler, I. J. The Role of the Organ Microenvironment in Brain Metastasis. *Semin. Cancer Biol.* **2011**, *21*, 107–112.

3. Lin, N. U.; Bellon, J. R.; Winer, E. P. CNS Metastases in Breast Cancer. *J. Clin. Oncol.* **2004**, *22*, 3608–3617.
4. Weil, R. J.; Palmieri, D. C.; Bronder, J. L.; Stark, A. M.; Steeg, P. S. Breast Cancer Metastasis to the Central Nervous System. *Am. J. Pathol.* **2005**, *167*, 913–920.
5. Gil-Gil, M. J.; Martinez-Garcia, M.; Sierra, A.; Conesa, G.; Del Barco, S.; Gonzalez-Jimenez, S.; Villa, S. Breast Cancer Brain Metastases: A Review of the Literature and a Current Multidisciplinary Management Guideline. *Clin. Transl. Oncol.* **2013**, *16*, 436–446.
6. Murrell, J.; Board, R. The Use of Systemic Therapies for the Treatment of Brain Metastases in Metastatic Melanoma: Opportunities and Unanswered Questions. *Cancer Treat. Rev.* **2013**, *39*, 833–838.
7. Wohlfart, S.; Gelperina, S.; Kreuter, J. Transport of Drugs across the Blood-Brain Barrier by Nanoparticles. *J. Controlled Release* **2012**, *161*, 264–273.
8. Tzeng, S. Y.; Green, J. J. Therapeutic Nanomedicine for Brain Cancer. *Ther. Delivery* **2013**, *4*, 687–704.
9. Wong, H. L.; Wu, X. Y.; Bendayan, R. Nanotechnological Advances for the Delivery of CNS Therapeutics. *Adv. Drug Delivery Rev.* **2012**, *64*, 686–700.
10. Reimold, I.; Domke, D.; Bender, J.; Seyfried, C. A.; Radunz, H. E.; Fricker, G. Delivery of Nanoparticles to the Brain Detected by Fluorescence Microscopy. *Eur. J. Pharm. Biopharm.* **2008**, *70*, 627–632.
11. Pardridge, W. M. Drug and Gene Targeting to the Brain with Molecular Trojan Horses. *Nat. Rev. Drug Discovery* **2002**, *1*, 131–139.
12. Jones, A. R.; Shusta, E. V. Blood−Brain Barrier Transport of Therapeutics *via* Receptor-Mediation. *Pharm. Res.* **2007**, *24*, 1759–1771.
13. Shah, L.; Yadav, S.; Amiji, M. Nanotechnology for Cns Delivery of Bio-Therapeutic Agents. *Drug Delivery Transl. Res.* **2013**, *3*, 336–351.
14. Ulbrich, K.; Knobloch, T.; Kreuter, J. Targeting the Insulin Receptor: Nanoparticles for Drug Delivery across the Blood-Brain Barrier (BBB). *J. Drug Targeting* **2011**, *19*, 125–132.
15. Ulbrich, K.; Hekmatara, T.; Herbert, E.; Kreuter, J. Transferrin- and Transferrin-Receptor-Antibody-Modified Nanoparticles Enable Drug Delivery across the Blood-Brain Barrier (BBB). *Eur. J. Pharm. Biopharm.* **2009**, *71*, 251–256.
16. Bertrand, Y.; Currie, J. C.; Demeule, M.; Regina, A.; Che, C.; Abulrob, A.; Fatehi, D.; Sartelet, H.; Gabathuler, R.; Castaigne, J. P.; *et al.* Transport Characteristics of a Novel Peptide Platform for CNS Therapeutics. *J. Cell Mol. Med.* **2010**, *14*, 2827–2839.
17. Wagner, S.; Zensi, A.; Wien, S. L.; Tschickardt, S. E.; Maier, W.; Vogel, T.; Worek, F.; Pietrzik, C. U.; Kreuter, J.; von Briesen, H. Uptake Mechanism of ApoE-Modified Nanoparticles on Brain Capillary Endothelial Cells as a Blood-Brain Barrier Model. *PLoS One* **2012**, *7*, e32568.
18. Gaillard, P. J.; Appeldoorn, C. C.; Rip, J.; Dorland, R.; van der Pol, S. M.; Kooij, G.; de Vries, H. E.; Reijerkerk, A. Enhanced Brain Delivery of Liposomal Methylprednisolone Improved Therapeutic Efficacy in a Model of Neuroinflammation. *J. Controlled Release* **2012**, *164*, 364–369.
19. Ren, T.; Xu, N.; Cao, C.; Yuan, W.; Yu, X.; Chen, J.; Ren, J. Preparation and Therapeutic Efficacy of Polysorbate-80-Coated Amphotericin B/Pla-B-Peg Nanoparticles. *J. Biomater. Sci., Polym. Ed.* **2009**, *20*, 1369–1380.
20. Kreuter, J.; Gelperina, S. Use of Nanoparticles for Cerebral Cancer. *Tumori* **2008**, *94*, 271–277.
21. Kreuter, J. Mechanism of Polymeric Nanoparticle-Based Drug Transport across the Blood-Brain Barrier (BBB). *J. Microencapsul.* **2013**, *30*, 49–54.
22. Powell, M. F.; Nguyen, T.; Baloian, L. Compendium of Excipients for Parenteral Formulations. *J. Pharm. Sci. Technol.* **1998**, *52*, 238–311.
23. Gulyaev, A. E.; Gelperina, S. E.; Skidan, I. N.; Antropov, A. S.; Kivman, G. Y.; Kreuter, J. Significant Transport of Doxorubicin into the Brain with Polysorbate 80-Coated Nanoparticles. *Pharm. Res.* **1999**, *16*, 1564–1569.
24. Ambruosi, A.; Gelperina, S.; Khalansky, A.; Tanski, S.; Theisen, A.; Kreuter, J. Influence of Surfactants, Polymer and Doxorubicin Loading on the Anti-Tumour Effect of Poly-(Butyl Cyanoacrylate) Nanoparticles in a Rat Glioma Model. *J. Microencapsul.* **2006**, *23*, 582–592.
25. Steiniger, S. C.; Kreuter, J.; Khalansky, A. S.; Skidan, I. N.; Bobruskin, A. I.; Smirnova, Z. S.; Severin, S. E.; Uhl, R.; Kock, M.; Geiger, K. D.; *et al.* Chemotherapy of Glioblastoma in Rats Using Doxorubicin-Loaded Nanoparticles. *Int. J. Cancer* **2004**, *109*, 759–767.
26. Kreuter, J.; Hekmatara, T.; Dreis, S.; Vogel, T.; Gelperina, S.; Langer, K. Covalent Attachment of Apolipoprotein a-I and Apolipoprotein B-100 to Albumin Nanoparticles Enables Drug Transport into the Brain. *J. Controlled Release* **2007**, *118*, 54–58.
27. Petri, B.; Bootz, A.; Khalansky, A.; Hekmatara, T.; Muller, R.; Uhl, R.; Kreuter, J.; Gelperina, S. Chemotherapy of Brain Tumour Using Doxorubicin Bound to Surfactant-Coated Poly(Butyl Cyanoacrylate) Nanoparticles: Revisiting the Role of Surfactants. *J. Controlled Release* **2007**, *117*, 51–58.
28. Hulsermann, U.; Hoffmann, M. M.; Massing, U.; Fricker, G. Uptake of Apolipoprotein E Fragment Coupled Liposomes by Cultured Brain Microvessel Endothelial Cells and Intact Brain Capillaries. *J. Drug Target.* **2009**, *17*, 610–618.
29. Huang, S.; Shao, K.; Liu, Y.; Kuang, Y.; Li, J.; An, S.; Guo, Y.; Ma, H.; Jiang, C. Tumor-Targeting and Microenvironment-Responsive Smart Nanoparticles for Combination Therapy of Antiangiogenesis and Apoptosis. *ACS Nano* **2013**, *7*, 2860–2871.
30. Miura, Y.; Takenaka, T.; Toh, K.; Wu, S.; Nishihara, H.; Kano, M. R.; Ino, Y.; Nomoto, T.; Matsumoto, Y.; Koyama, H.; *et al.* Cyclic Rgd-Linked Polymeric Micelles for Targeted Delivery of Platinum Anticancer Drugs to Glioblastoma through the Blood-Brain Tumor Barrier. *ACS Nano* **2013**, *7*, 8583–8592.
31. Deeken, J. F.; Loscher, W. The Blood-Brain Barrier and Cancer: Transporters, Treatment, and Trojan Horses. *Clin. Cancer. Res.* **2007**, *13*, 1663–1674.
32. Choi, M.-R.; Bardhan, R.; Stanton-Maxey, K.; Badve, S.; Nakshatri, H.; Stantz, K.; Cao, N.; Halas, N.; Clare, S. Delivery of Nanoparticles to Brain Metastases of Breast Cancer Using a Cellular Trojan Horse. *Cancer Nano.* **2012**, *3*, 47–54.
33. Shalviri, A.; Chan, H. K.; Raval, G.; Abdekhodaie, M. J.; Liu, Q.; Heerklotz, H.; Wu, X. Y. Design of pH-Responsive Nanoparticles of Terpolymer of Poly (Methacrylic Acid), Polysorbate 80 and Starch for Delivery of Doxorubicin. *Colloids Surf., B* **2013**, *101*, 405–413.
34. Shalviri, A.; Foltz, W. D.; Cai, P.; Rauth, A. M.; Wu, X. Y. Multifunctional Terpolymeric MRI Contrast Agent with Superior Signal Enhancement in Blood and Tumor. *J. Controlled Release* **2013**, *167*, 11–20.
35. Shalviri, A.; Cai, P.; Rauth, A. M.; Henderson, J. T.; Wu, X. Y. Evaluation of New Bi-Functional Terpolymeric Nanoparticles for Simultaneous *in Vivo* Optical Imaging and Chemotherapy of Breast Cance. *Drug Delivery Transl. Res.* **2012**, *2*, 437–453.
36. Shalviri, A.; Raval, G.; Prasad, P.; Chan, C.; Liu, Q.; Heerklotz, H.; Rauth, A. M.; Wu, X. Y. pH Dependent Doxorubicin Release from Terpolymer of Starch, Polymethacrylic Acid and Polysorbate 80 Nanoparticles for Overcoming Multi-Drug Resistance in Human Breast Cancer Cells. *Eur. J. Pharm. Biopharm.* **2012**, *82*, 587–597.
37. Koffie, R. M.; Farrar, C. T.; Saidi, L.-J.; William, C. M.; Hyman, B. T.; Spires-Jones, T. L. Nanoparticles Enhance Brain Delivery of Blood−Brain Barrier-Impermeable Probes for *in vivo* Optical and Magnetic Resonance Imaging. *Proc. Natl. Acad. Sci. U.S.A.* **2011**, *108*, 18837–18842.
38. Verreault, M.; Strutt, D.; Masin, D.; Anantha, M.; Yung, A.; Kozlowski, P.; Waterhouse, D.; Bally, M. B.; Yapp, D. T. Vascular Normalization in Orthotopic Glioblastoma Following Intravenous Treatment with Lipid-Based Nanoparticulate Formulations of Irinotecan (Irinophore C), Doxorubicin (Caelyx(R)) or Vincristine. *BMC Cancer* **2011**, *11*, 124.
39. Hans, M. L.; Lowman, A. M. Biodegradable Nanoparticles for Drug Delivery and Targeting. *Curr. Opin. Solid State Mater. Sci.* **2002**, *6*, 319–327.

40. Lockman, P. R.; Koziara, J. M.; Mumper, R. J.; Allen, D. D. Nanoparticle Surface Charges Alter Blood-Brain Barrier Integrity and Permeability. *J. Drug Targeting* **2004**, *12*, 635–641.
41. Morelli, J. N.; Runge, V. M.; Ai, F.; Attenberger, U.; Vu, L.; Schmeets, S. H.; Nitz, W. R.; Kirsch, J. E. An Image-Based Approach to Understanding the Physics of MR Artifacts. *Radiographics* **2011**, *31*, 849–866.
42. Schnell, S. A.; Staines, W. A.; Wessendorf, M. W. Reduction of Lipofuscin-Like Autofluorescence in Fluorescently Labeled Tissue. *J. Histochem. Cytochem.* **1999**, *47*, 719–730.
43. Lin, N. U.; Claus, E.; Sohl, J.; Razzak, A. R.; Arnaout, A.; Winer, E. P. Sites of Distant Recurrence and Clinical Outcomes in Patients with Metastatic Triple-Negative Breast Cancer: High Incidence of Central Nervous System Metastases. *Cancer* **2008**, *113*, 2638–2645.
44. Lin, N. U.; Winer, E. P. Brain Metastases: The HER2 Paradigm. *Clin. Cancer Res.* **2007**, *13*, 1648–1655.
45. Dent, R.; Trudeau, M.; Pritchard, K. I.; Hanna, W. M.; Kahn, H. K.; Sawka, C. A.; Lickley, L. A.; Rawlinson, E.; Sun, P.; Narod, S. A. Triple-Negative Breast Cancer: Clinical Features and Patterns of Recurrence. *Clin. Cancer Res.* **2007**, *13*, 4429–4434.
46. Hammond, M. E.; Hayes, D. F.; Dowsett, M.; Allred, D. C.; Hagerty, K. L.; Badve, S.; Fitzgibbons, P. L.; Francis, G.; Goldstein, N. S.; Hayes, M.; *et al.* American Society of Clinical Oncology/College of American Pathologists Guideline Recommendations for Immunohistochemical Testing of Estrogen and Progesterone Receptors in Breast Cancer. *J. Clin. Oncol.* **2010**, *28*, 2784–2795.
47. Kreuter, J.; Shamenkov, D.; Petrov, V.; Ramge, P.; Cychutek, K.; Koch-Brandt, C.; Alyautdin, R. Apolipoprotein-Mediated Transport of Nanoparticle-Bound Drugs across the Blood-Brain Barrier. *J. Drug Targeting* **2002**, *10*, 317–325.
48. Saito, N.; Hatori, T.; Murata, N.; Zhang, Z.-A.; Nonaka, H.; Aoki, K.; Iwabuchi, S.; Ueda, M. Comparison of Metastatic Brain Tumour Models Using Three Different Methods: The Morphological Role of the Pia Mater. *Int. J. Exp. Pathol.* **2008**, *89*, 38–44.
49. Daphu, I.; Sundstrom, T.; Horn, S.; Huszthy, P. C.; Niclou, S. P.; Sakariassen, P. O.; Immervoll, H.; Miletic, H.; Bjerkvig, R.; Thorsen, F. *in vivo* Animal Models for Studying Brain Metastasis: Value and Limitations. *Clin. Exp. Metastasis* **2013**, *30*, 695–710.
50. American Brain Tumor Association. Metastatic Brain Tumors [Online], 2012. http://www.abta.org/secure/metastatic-brain-tumor.pdf.
51. Misra, A.; Ganesh, S.; Shahiwala, A.; Shah, S. P. Drug Delivery to the Central Nervous System: A Review. *J. Pharm. Pharm. Sci.* **2003**, *6*, 252–273.
52. Vermeulen, K.; Van Bockstaele, D. R.; Berneman, Z. N. Apoptosis: Mechanisms and Relevance in Cancer. *Ann. Hematol.* **2005**, *84*, 627–639.
53. Liebner, S.; Fischmann, A.; Rascher, G.; Duffner, F.; Grote, E. H.; Kalbacher, H.; Wolburg, H. Claudin-1 and Claudin-5 Expression and Tight Junction Morphology Are Altered in Blood Vessels of Human Glioblastoma Multiforme. *Acta. Neuropathol.* **2000**, *100*, 323–331.
54. Regina, A.; Demeule, M.; Laplante, A.; Jodoin, J.; Dagenais, C.; Berthelet, F.; Moghrabi, A.; Beliveau, R. Multidrug Resistance in Brain Tumors: Roles of the Blood-Brain Barrier. *Cancer Metastasis Rev.* **2001**, *20*, 13–25.
55. Wohlfart, S.; Khalansky, A. S.; Bernreuther, C.; Michaelis, M.; Cinatl, J., Jr.; Glatzel, M.; Kreuter, J. Treatment of Glioblastoma with Poly(Isohexyl Cyanoacrylate) Nanoparticles. *Int. J. Pharm.* **2011**, *415*, 244–251.